

https://doi.org/10.1070/QEL17154

Tapered erbium-doped fibre laser system delivering 10 MW of peak power

A.V. Andrianov, M.Yu. Koptev, E.A. Anashkina, S.V. Muravyev, A.V. Kim, D.S. Lipatov, V.V. Velmiskin, A.E. Levchenko, M.M. Bubnov, M.E. Likhachev

Abstract. **We consider a fibre laser system generating ~10-μJ, ~500-fs pulses with a peak power of ~10 MW at a repetition rate of 100 kHz and emission wavelength of 1.56 μm. The system is based on a master oscillator–power amplifier configuration. The amplifier ensures chirped-pulse amplification. The pulses are then compressed by a dispersive grating compressor. The output amplifier stage is based on a specially designed tapered large mode area erbium-doped fibre for suppressing nonlinear effects. The experimental data agree with numerical simulation results for the stretcher, amplifier and compressor. The stretcher and amplifier have been simulated using a generalised nonlinear Schrödinger equation. In addition, numerical simulation results suggest that optimising the stretcher and compressor will potentially allow the peak power of the system to be scaled up to ~30 MW.**

Keywords: *high peak power fibre laser systems, chirped-pulse amplification, erbium-doped fibre amplifiers, tapered fibre, dispersive grating compressor.*

1. Introduction

Recent advances in high peak power pulsed fibre laser systems are in large measure due to the fact that such systems are highly demanded in both basic research and practical applications, among which it is worth noting materials processing, biomedicine, nonlinear spectroscopy etc. At present, laser systems operating at wavelengths in the 1.5 μm range and utilising erbium-doped active silica fibre and well-developed telecom fibre-optic components find wide application [1]. Fibre laser systems are characterised by high diode pump to signal energy conversion efficiency due to their guiding geometry, the possibility of effective heat dissipation, the high quality of the spatial beam profile and their relatively low cost, in combination with their good weight and size parameters. Because of this, a great deal of attention is being paid to the development and optimisation of fibre laser systems.

The fabrication of high-power fibre laser systems is often based on the use of a standard master oscillator–power amplifier configuration [1]. Since the energy and peak power of pulses in such systems are often limited by not only the diode pump power but also the active fibre nonlinearity in the output amplifier stage, chirped-pulse amplification is used to reach high energies [2] and external dispersive compressors based on bulk elements, such as prisms, diffraction gratings or their combinations, are used for frequency modulation compensation [1, 3]. To suppress nonlinear effects, use is also made of large mode area (LMA) fibre, which allows one to obtain high-energy, high peak power pulses [4–7]. However, when using LMA fibres, which are usually multimode, one encounters the problem of suppressing higher order modes. The problem can be resolved by utilising tapered fibre which is sufficiently thin at its input end for single-mode signal propagation at the input and expands towards its output end [8]. An adiabatic increase in the diameter of a tapered active fibre ensures quasi-single-mode signal propagation throughout its length, making it possible to maintain high beam quality and reduce the nonlinear phase shift (obtain a relatively small B-integral).

In this paper, we consider a fibre laser system based on a specially designed tapered large mode area erbium-doped fibre for suppressing nonlinear effects, which employs chirped-pulse amplification and subsequent pulse compression by a dispersive grating compressor. The system makes it possible to reach a pulse peak power of ~10 MW, which exceeds the critical power for self-focusing in glass, as confirmed by relevant experimental data. The experimental data agree with numerical simulation results for the stretcher, amplifier and compressor. In numerical simulations of broadband amplifiers, we use a calibrated model based on a generalised nonlinear Schrödinger equation. In addition, numerical simulation results demonstrate that optimising only the stretcher and compressor allows the peak power of the system to be scaled up to ~30 MW.

2. Tapered erbium-doped fibre

A silica preform for tapered active fibre with an erbium-doped core was produced by MCVD, an all-gas-phase process. To reduce the degree of erbium clustering and ensure a small core–cladding refractive index difference, the core was additionally doped with phosphorus and aluminium oxides.

A.V. Andrianov, M.Yu. Koptev, E.A. Anashkina, S.V. Muravyev, A.V. Kim Institute of Applied Physics (Federal Research Centre), Russian Academy of Sciences, ul. Ul'yanova 46, 603950 Nizhny Novgorod, Russia; e-mail: alex.v.andrianov@gmail.com;
D.S. Lipatov Devyatykh Institute of Chemistry of High-Purity Substances, Russian Academy of Sciences, ul. Tropinina 49, 603950 Nizhny Novgorod, Russia;
V.V. Velmiskin, A.E. Levchenko, M.M. Bubnov, M.E. Likhachev Fiber Optics Research Center, Russian Academy of Sciences, ul. Vavilova 38, 119333 Moscow, Russia

Received 10 October 2019
Kvantovaya Elektronika **49** (12) 1093–1099 (2019)
Translated by O.M. Tsarev

The erbium oxide concentration in the core was ~0.14 mol %. After polishing, the preform had a square cross section for better pump absorption and was coated with fluorinated silica glass. Next, the preform was drawn into tapered fibre. Figure 1a shows the refractive index profile of the tapered fibre at a point corresponding to a diameter of 110 μm, and Fig. 1b shows an optical micrograph of its end face. The numerical aperture at the pump wavelength (976 nm) was ~0.3. The ratio of the core diameter to the inner cladding diameter was taken to be 1/3 to ensure better pump absorption.

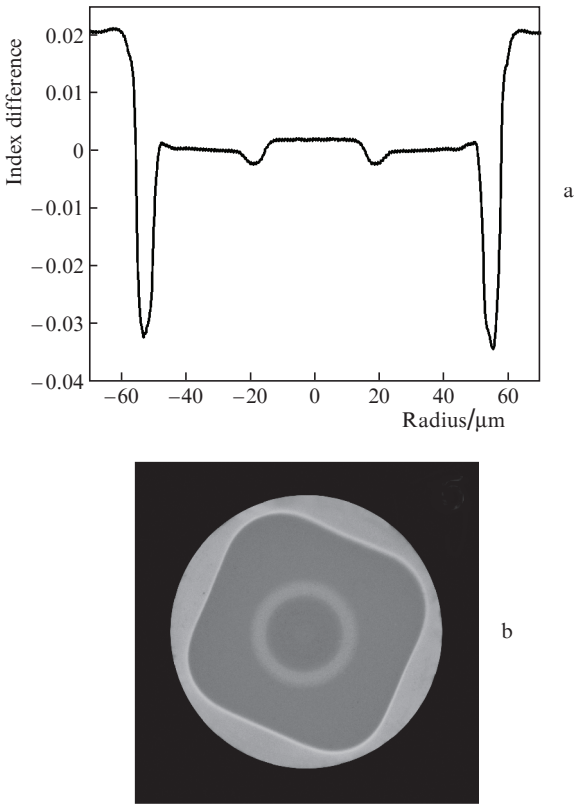

Figure 1. (a) Refractive index profile of the 110-μm-diameter tapered erbium-doped fibre and (b) micrograph of its cross section.

To make a high-power fibre laser system, we used a 3.2-m length of tapered fibre with an initial cladding diameter of 88 μm and a final diameter of 300 μm. The longitudinal fibre diameter profile is shown in Fig. 2. The core diameter varied from 22 μm at the input end to 75 μm at the output end. The maximum experimentally measured small-signal cladding pump absorption at a wavelength of 976 nm was 4 dB m^{-1} (Fig. 3). The relatively weak pump absorption significantly limits the efficiency of short tapered erbium-doped fibres and raises requirements for the pump power needed to reach a particular output power. This, however, is not an obstacle to obtaining high-energy, high peak power pulses in amplifiers having such tapered fibre in their output stage.

3. Experimental implementation of the laser system

Figure 4 shows a schematic of the experimental setup. Its key component is a previously designed ring-cavity erbium-

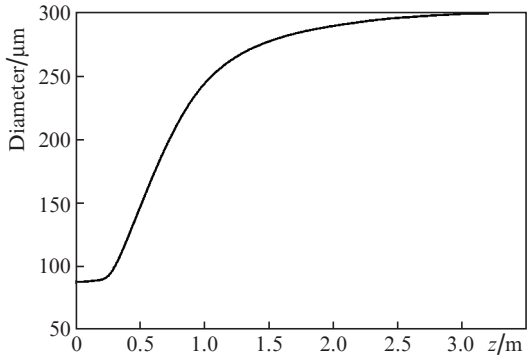

Figure 2. Tapered fibre diameter as a function of the longitudinal coordinate z.

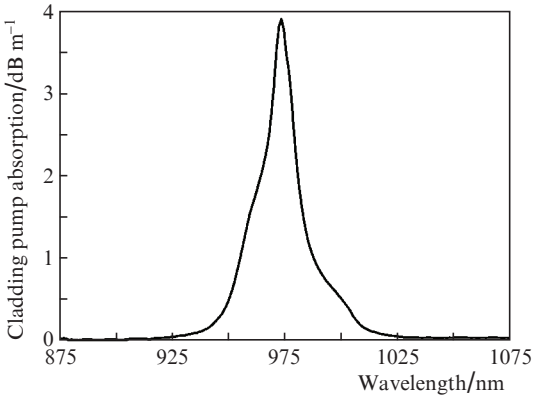

Figure 3. Small-signal cladding pump absorption in the tapered erbium-doped fibre.

doped fibre laser diode-pumped at a wavelength of 976 nm. The laser is passively mode-locked via nonlinear rotation of the polarisation ellipse of a femtosecond pulse due to the optical Kerr effect. The master oscillator generates 230-fs pulses at a repetition rate of 50 MHz and a wavelength of 1.56 μm [9–11]. After it, the scheme contains a Faraday isolator and a fibre stretcher. The fibre stretcher has a double-pass configuration and is based on a 160-m length of germanosilicate fibre with a group velocity dispersion of –54 ps nm^{-1} km^{-1} at a wavelength of 1.56 μm. The double-pass configuration is ensured by a Faraday mirror placed at the end of the stretcher, and a fibre polarisation splitter is used to separate the input and output beams. Owing to the double-pass configuration, the effective stretcher length is 320 m. This design allows undesirable birefringence to be avoided as well.

The next component of the scheme is an erbium-doped fibre preamplifier diode-pumped in a copropagating configuration. It increases the average power to 100 mW, which corresponds to a pulse energy of 2 nJ. The pulse train is then decimated by an acousto-optic modulator to a repetition rate of 100 kHz and again amplified in the second preamplifier, also diode-pumped by a copropagating beam, to an average power of ~1 mW, which corresponds to a pulse energy of ~10 nJ. After it, the scheme contains a tapered fibre-based output amplifier stage. Since the tapered fibre is few-mode in its thin part, its initial portion is coiled at a diameter of ~10 cm. This allows for quasi-single-mode signal propagation in this part of the fibre. An adiabatic increase in fibre

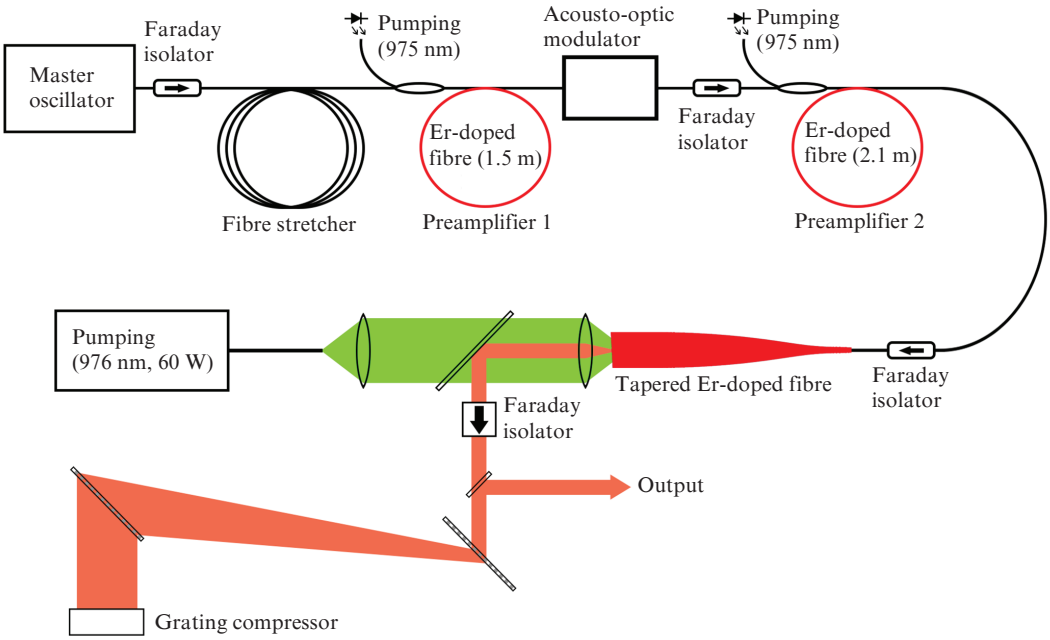

Figure 4. Schematic of the erbium-doped fibre laser system.

diameter allows quasi-single-mode signal propagation to be retained throughout the length of the tapered fibre.

The tapered fibre is cladding-pumped in a counterpropagating pump and signal configuration. To this end, we use a 60-W multimode laser diode (IPG Photonics, PLD-70) with a stabilised emission wavelength of 976 nm. The signal is outcoupled using a dichroic dielectric mirror. The tapered fibre is protected against back-reflections by a bulk Faraday isolator placed after the amplifier. The maximum average power of the signal at the output of the final amplifier stage is 1.3 W. Figure 5 shows the spectrum of pulses at the output of the tapered fibre.

For frequency modulation compensation and amplified pulse compression, we use a compressor based on a pair of polarisation-insensitive transmissive diffraction gratings (LightSmyth, T-940CL, 940 lines mm^{-1}). The grating separation is ~48 cm, and the angle of incidence (between the normal to the grating and the beam propagation direction) is 47.5°. The pulse duration at the compressor output is ~500 fs, but part of the signal lies in the pulse pedestal because of the uncompensated higher order dispersion. The intensity distribution of amplified and compressed signals was measured using a previously designed computer-controlled frequency-resolved optical gating (FROG) system [12, 13]. Figure 6 shows a signal intensity profile reconstructed using an iteration algorithm and the inset in Fig. 6 shows an experimentally measured FROG trace, which has the form of a set of spectra

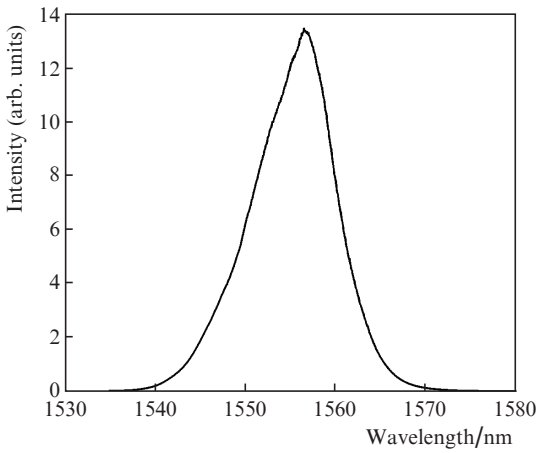

Figure 5. Experimentally measured spectrum of the signal at the output of the tapered erbium-doped fibre.

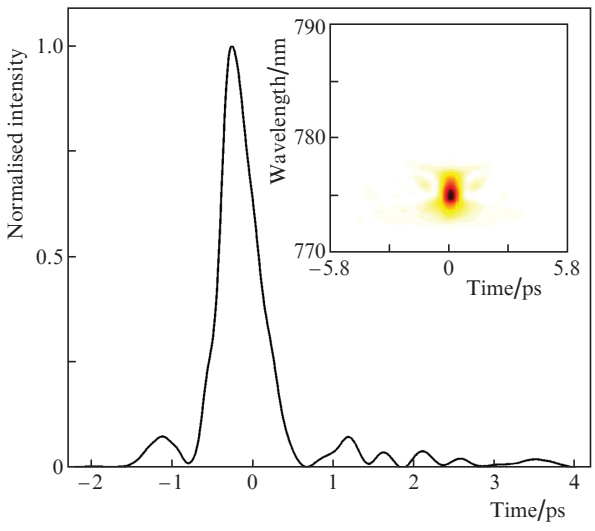

Figure 6. Pulse intensity profile at the output of the fibre laser system, retrieved by the frequency-resolved optical gating technique from the experimentally measured FROG trace shown in the inset.

of the sum harmonic at different time delays between replicas of the signal being measured.

The pulse peak power at the output of the erbium-doped fibre laser system, P_{peak}, estimated with allowance for the pedestal of the reconstructed signal, is ~10 MW, exceeding the critical power for self-focusing, P_{cr}, in glass ($P_{peak} \approx 1.3P_{cr}$). To experimentally confirm this, pulses from the output of the laser system were focused by a long-focus lens into a 7-cm-long BK7 glass rod. In addition, the light exhibited self-focusing, accompanied by severe broadening of the spectrum and supercontinuum generation in the visible spectral region (Fig. 7). Moreover, the power of the system was sufficient for estimating peak power and pulse duration fluctuations in single-shot mode [14].

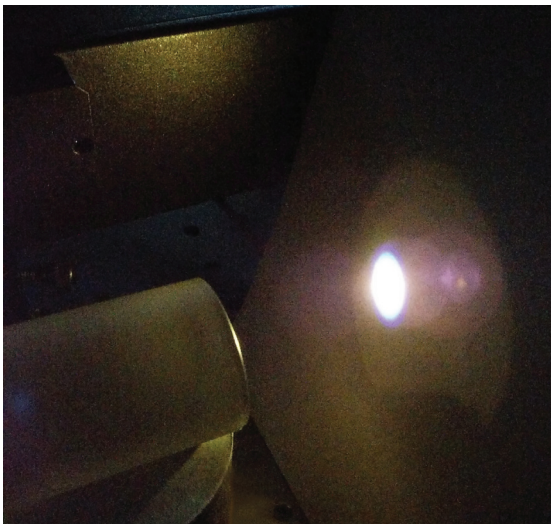

Figure 7. Photograph of supercontinuum light resulting from self-focusing of the output beam of the erbium system in glass.

4. Numerical simulation and optimisation of the laser system

Signal propagation in three amplifier stages was simulated using real parameters of the laser system schematised in Fig. 4.

Let $E(z,t)$ be the complex pulse field amplitude, z be a coordinate along the fibre, t be the time in a moving frame of reference, and $\tilde{E}(z,\omega)$ be the Fourier transform of the function $E(z,t)$, defined through the Fourier transform operator $\hat{F}$:

$$\tilde{E}(z,\omega) = \hat{F}[E(z,t)], \tag{1}$$

where $\omega = 2\pi c/\lambda$ is the angular frequency; λ is the wavelength; and c is the speed of light in vacuum. The mathematical model of the amplifiers relies on a generalised nonlinear Schrödinger equation for the complex field amplitude of pulses propagating in the LP_{01} fundamental mode of the fibre [15]. A model of broadband amplifiers based on rare-earth-doped fibre was constructed, investigated and calibrated using experimental data in previous work. It was described in detail elsewhere [16–21]. To find a solution to the Schrödinger equation, other numerical schemes can be used [22]. The nonlinear Schrödinger equation can be written in the frequency domain as follows:

$$\frac{\partial\tilde{E}(z,\omega)}{\partial z} - \mathrm{i}\gamma\hat{F}\left[E(z,t)\int R(t-\tau)\,|E(z,\tau)|^2\,\mathrm{d}\tau\right] + \mathrm{i}\beta\tilde{E}(z,\omega) = \frac{g(\omega)}{2}\tilde{E}(z,\omega), \tag{2}$$

where β is the propagation constant; γ is the Kerr nonlinearity coefficient; $R(t-\tau)$ is the Raman response function [15]; and $g(\omega)$ is the gain function calculated with allowance for the measured emission and absorption cross sections of silica fibre [23]. The nonlinearity coefficient is given by [15]

$$\gamma = \frac{n_2\omega}{cA_{eff}}, \tag{3}$$

where n_2 is the nonlinear refractive index ($n_2 = 2.5 \times 10^{-20}$ m^2 W^{-1} [15]);

$$A_{eff} = \frac{\left[\int_0^\infty |F(r,\omega)|^2 2\pi r\mathrm{d}r\right]^2}{\int_0^\infty |F(r,\omega)|^4 2\pi r\mathrm{d}r} \tag{4}$$

is the effective mode area calculated for axisymmetric refractive index profiles of fibre; r is a radial coordinate; and $F(r,\omega)$ is the electric field of the LP_{01} mode [15].

We calculated fundamental mode fields at different core diameters of the tapered fibre. To this end, we solved the problem of the eigenvalues and eigenfunctions of the Helmholtz equation [24] and then, using relation (3), estimated nonlinearity coefficients, which were used in nonlinear pulse amplification simulation. Since the fibre core has a rather large diameter, the waveguide contribution to the dispersion is small, and the dispersion of the tapered fibre is essentially determined by that of the fibre material. In our simulations, the dispersion of the fibre was taken to be equal to that of silica glass at any fibre diameter [15].

In modelling Eqn (1), we used the split-step Fourier method (SSFM) [15], fast Fourier transformation (FFT) and inverse FFT. The step along the fibre axis, dz, was taken to be 100 μm. We ascertained that a factor of 2 reduction in step had no effect on simulation results.

In simulating the compressor, we used a standard method based on ray tracing at various wavelengths and neglected diffraction-limited beam divergence [25].

Figure 8 presents the numerical simulation results obtained for the stretcher–three-stage amplifier–compressor system with allowance for its real parameters. The calculated signals at the output of the final stage were 130 ps in duration, with a spectral width corresponding to 360 fs, and their energy was 15 μJ. Compression was assumed to reduce the pulse energy to 10 μJ, which corresponded to our experimental data (due to the finite grating efficiency and the loss in the bulk Faraday isolator represented in the schematic in Fig. 4 at the output of the tapered fibre). The B-integral was determined to be 4. Figure 8a shows the calculated signal peak power as a function of the separation L between the gratings of the compressor, and Fig. 8b shows the pulse

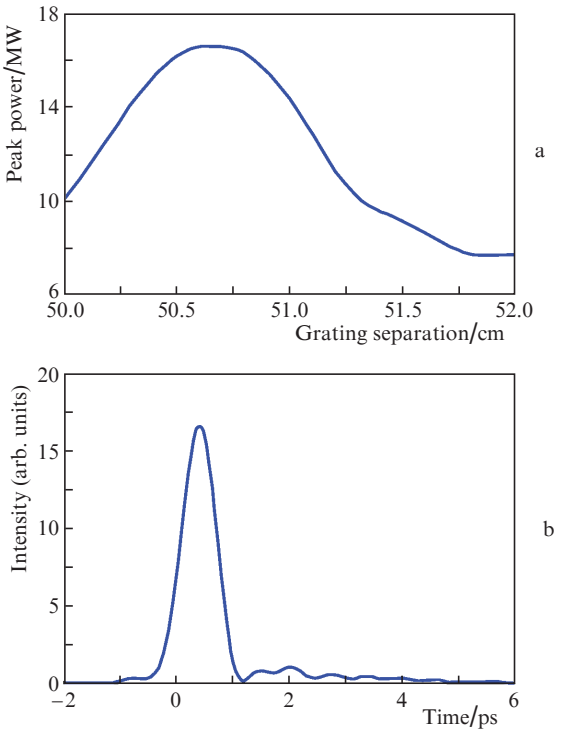

Figure 8. (a) Pulse peak power at the output of the laser system calculated using its real parameters as a function of the separation L between the gratings of the dispersive compressor and (b) calculated pulse intensity profile at the optimal grating separation $L = 50.6$ cm.

intensity profile at the optimal grating separation L = 50.6 cm. The numerical simulation results are seen to be, on the whole, in rather good agreement with the present experimental data, but in the case optimal for the compressor, the signal pedestal is smaller and the peak power is slightly higher than those in the case of the FROG-retrieved pulses shown in Fig. 6.

In addition, we theoretically examined the feasibility of optimising the stretcher–compressor system via precompensation for higher order dispersion parameters in the stretcher. In experiments, this can be achieved, for example, using a stretcher based on a specially designed fibre with desired parameters or chirped Bragg gratings with required dispersion coefficients. Note that, with modern technologies, both approaches can, in principle, be implemented. Signal compression is assumed to be ensured by available gratings. On the one hand, the larger the signal chirp, the lower the peak power in the amplifier, the smaller nonlinear phase shift (B-integral), and the stronger pulse compression in the compressor. On the other hand, there is a limitation on the maximum separation between the gratings, related to their size and the spectral width of the amplified signal: starting at some grating separation, the wings of the spectrum are 'cut off', which leads to a decrease in energy and compressed signal quality degradation.

We examined the feasibility of increasing the grating separation by a factor of ~2 in comparison with the experimental value. Figure 9 presents simulation results for two cases. In one of them, dispersion parameters of up to the fourth order are precompensated, i.e. the coefficients β_2, β_3 and β_4 are optimised for the stretcher. In the other (considered for comparison), only the coefficient β_2 is optimised, and we take $\beta_3 = 0$ and $\beta_4 = 0$. Figures 9a and 9b show calculated spectra of the signal before the stretcher, after the first and second preamplifiers and after the output amplifier stage. In addition, Figs 9a and 9b show calculated spectral phases at the tapered fibre output. The observed narrowing of the spectrum after each stage is due to the finite gain bandwidth. Figures 9c and 9d show pulse intensity profiles after the output stage. In the case of dispersion precompensation up to the fourth order, we find $\beta_2 = 33.8$ ps^2, $\beta_3 = -0.2606$ ps^3 and $\beta_4 = -0.0196$ ps^4. In addition, the duration of the amplified chirped signal after the output stage is 183.7 ps, and the spectral width corresponds to 361 fs. The B-integral is 2.833. If only the second-order dispersion is precompensated, with $\beta_2 = 34$ ps^2, $\beta_3 = 0$ and $\beta_4 = 0$, the duration of the amplified chirped signal after the output stage is 185.2 ps, at the same spectral width. The B-integral is 2.807. Figures 9e and 9f show the peak power as a function of the separation between the gratings of the compressor, L, and Figs 9g and 9h show pulse intensity profiles at the optimal grating separation $L = 93.1$ cm. It is seen that the precompensation of dispersion parameters up to the fourth order makes it possible to obtain shorter, near transform-limited pulses with a smaller pedestal and, hence, higher peak power – up to ~30 MW.

5. Conclusions

We have considered a fibre laser system generating ~10-μJ ultrashort pulses at a repetition rate of 100 kHz and emission wavelength of 1.56 μm. The system is based on a master oscillator–power amplifier configuration. The master oscillator is passively mode-locked via polarisation ellipse rotation due to the optical Kerr effect and generates 230-fs pulses. The signal is chirped before the amplifier to an ~100 ps duration in normal-dispersion fibre. The three-stage amplifier ensures chirped-pulse amplification. The pulses are then compressed by a dispersive compressor in the form of a grating pair. The output amplifier stage is based on a specially designed tapered large mode area erbium-doped fibre for suppressing nonlinear effects. Even though the tapered fibre is multimode at its output (the core diameter varies from 22 μm at the fibre input to 75 μm at the output), quasi-single-mode amplification can be achieved. The output pulse duration (~500 fs) has been determined by the frequency-resolved optical gating technique. The peak power has been estimated at ~10 MW, which exceeds the critical power for self-focusing in glass and is confirmed by relevant experimental data.

The present experimental data agree with numerical simulation results for a fibre stretcher, three-stage amplifier and compressor. The stretcher and amplifier have been simulated using a generalised nonlinear Schrödinger equation. In addition, numerical simulation results suggest that optimising the stretcher and compressor will potentially allow the peak power of the system to be scaled up to ~30 MW.

Acknowledgements. This work was supported in part by the Presidium of the Russian Academy of Sciences (Extreme Light Fields and Their Interaction with Matter Programme). The development of the tapered erbium-doped fibre was supported by the Russian Science Foundation (Grant No. 16-12-10553).

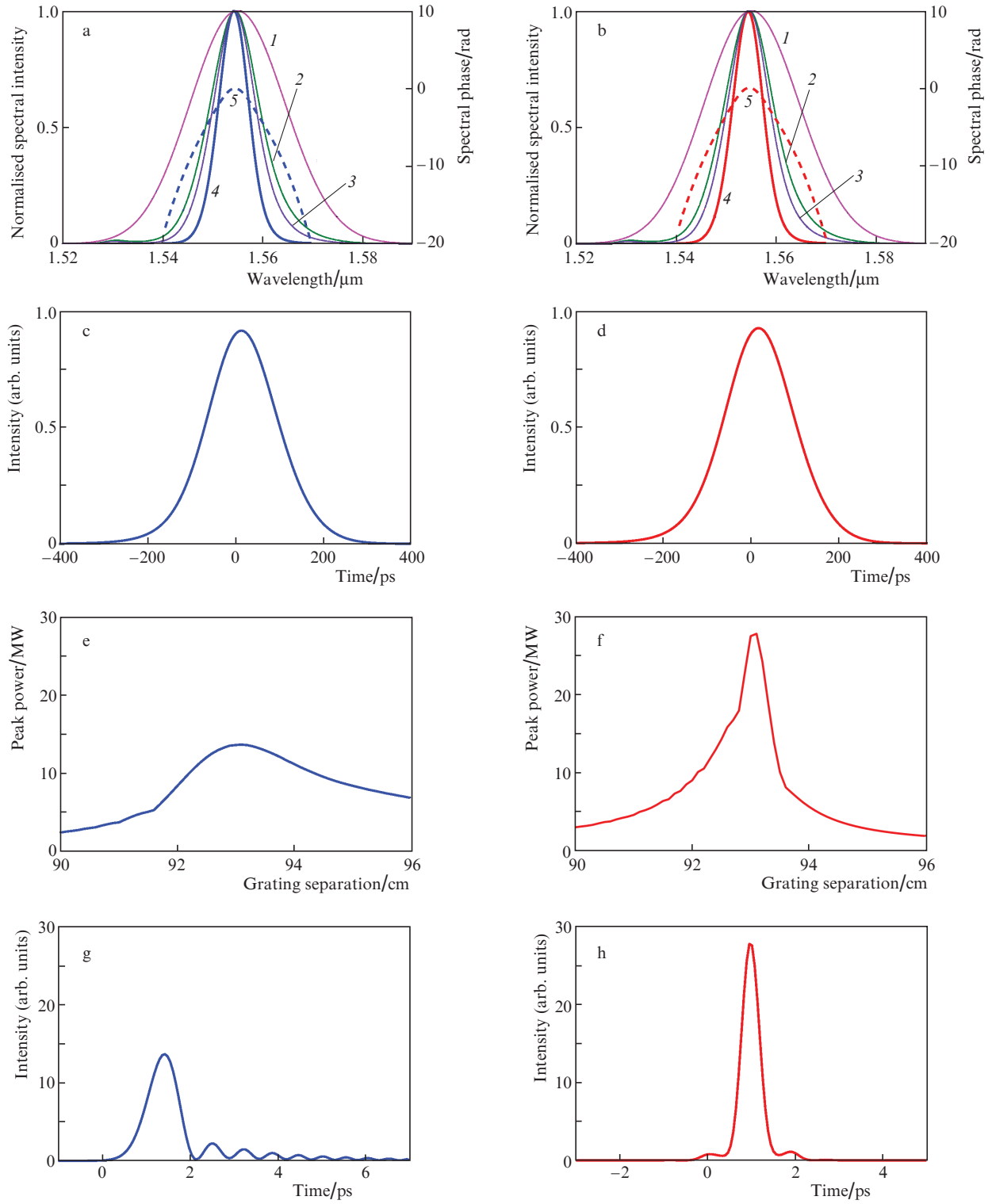

Figure 9. Calculated spectra of the signal before the stretcher (*1*), after the first (*2*) and second (*3*) preamplifiers and after the output amplifier stage [(*4*) spectrum, (*5*) spectral phase] in the case of (a) precompensation for only the second-order dispersion β_2 in the stretcher and (b) precompensation for dispersion coefficients of up to the fourth order: β_2, β_3 and β_4. Calculated amplified pulse profiles at the tapered fibre output in the case of precompensation (c) for only β_2 and (d) for β_2, β_3 and β_4. Calculated pulse peak power as a function of the separation between the gratings of the dispersive compressor, L, in the case of precompensation (e) for only β_2 and (f) for β_2, β_3 and β_4. Pulse intensity profile at the optimal grating separation $L = 93.1$ cm in the case of precompensation (g) for only β_2 and (h) for β_2, β_3 and β_4.

References

1. Richardson D.J., Nilsson J., Clarkson W.A. *J. Opt. Soc. Am. B*, **27**, B63 (2010).
2. Strickland D., Mourou G. *Opt. Commun.*, **55**, 447 (1985).
3. Fermann M.E., Galvanauskas A., Sucha G., Harter D. *Appl. Phys. B*, **65**, 259 (1997).

4. Taverner D., Richardson D.J., Dong L., Caplen J.E., Williams K., Penty R.V. *Opt. Lett*., **22**, 378 (1997).
5. Lim E.-L., Alam S., Richardson D.J. *Opt. Express*, **20**, 18803 (2012).
6. Jasapara J.C., Andrejco M.J., DeSantolo A., Yablon A.D., Varallyay Z., Nicholson J.W., Fini J.M., DiGiovanni D.J., Headley C., Monberg E., DiMarcello F.V. *IEEE J. Sel. Top. Quantum Electron*., **15**, 3 (2009).
7. Kotov L.V., Koptev M.Yu., Anashkina E.A., Muravyev S.V., Andrianov A.V., Bubnov M.M., Ignat'ev A.D., Lipatov D.S., Gur'yanov A.N., Likhachev M.E., Kim A.V. *Quantum Electron*., **44**, 458 (2014) [*Kvantovaya Elektron*., **44**, 458 (2014)].
8. Bobkov K., Andrianov A., Koptev M., Muravyev S., Levchenko A., Velmiskin V., Aleshkina S., Semjonov S., Lipatov D., Guryanov A., Kim A., Likhachev M. *Opt. Express*, **25**, 26958 (2017).
9. Andrianov A., Kim A., Muraviov S., Sysoliatin A. *Opt. Lett*., **34**, 3193 (2009).
10. Koptev M.Yu., Anashkina E.A., Bobkov K.K., Likhachev M.E., Levchenko A.E., Aleshkina S.S., Semjonov S.L., Denisov A.N., Bubnov M.M., Lipatov D.S., Laptev A.Yu., Gur'yanov A.N., Andrianov A.V., Muravyev S.V., Kim A.V. *Quantum Electron*., **45**, 443 (2015) [*Kvantovaya Elektron*., **45**, 443 (2015)].
11. Anashkina E.A., Shiryaev V.S., Koptev M.Y., Stepanov B.S., Muravyev S.V. *J. Non-Cryst. Solids*, **480**, 43 (2018).
12. Anashkina E.A., Andrianov A.V., Koptev M.Yu., Kim A.V. *IEEE J. Sel. Top. Quantum Electron*., **24**, 8700107 (2018).
13. Anashkina E.A., Koptev M.Y., Andrianov A.V., Dorofeev V.V., Singh S., Leuchs G., Kim A.V. *J. Lightwave Technol*., **37**, 43751 (2019).
14. Andrianov A.V., Anashkina E.A., Koptev M.Yu., Kim A.V. *Quantum Electron*., **49**, 322 (2019) [*Kvantovaya Elektron*., **49**, 322 (2019)].
15. Agrawal G.P. *Nonlinear Fiber Optics* (Waltham: Academic Press, 2013).
16. Anashkina E.A., Dorofeev V.V., Muravyev S.V., Motorin S.E., Andrianov A.V., Sorokin A.A., Koptev M.Yu., Singh S., Kim A.V. *Quantum Electron*., **48**, 1118 (2018) [*Kvantovaya Elektron*., **48**, 1118 (2018)].
17. Anashkina E.A., Andrianov A.V., Dorofeev V.V., Muravyev S.V., Koptev M.Y., Sorokin A.A., Motorin S.E., Koltashev V.V., Galagan B.I., Denker B.I. *Laser Phys. Lett*., **16**, 025107 (2019).
18. Anashkina E.A., Kim A.V. *J. Lightwave Technol*., **35**, 5397 (2017).
19. Muravyev S.V., Anashkina E.A., Andrianov A.V., Dorofeev V.V., Motorin S.E., Koptev M.Yu., Kim A.V. *Sci. Rep*., **8**, 16164 (2018).
20. Anashkina E.A., Andrianov A.V., Dorofeev V.V., Kim A.V., Koltashev V.V., Leuchs G., Motorin S.E., Muravyev S.V., Plekhovich A.D. *J. Non-Cryst. Solids*, **525**, 119667 (2019).
21. Andrianov A., Anashkina E., Kim A., Meyerov I., Lebedev S., Sergeev A., Mourou G. *Opt. Express*, **22**, 28256 (2014).
22. Sujecki S., Sojka L., Seddon A.B., Benson T.M., Barney E., Falconi M.C., Prudenzano F., Marciniak M., Baghdasaryan H., Peterka P., Taccheo S. *Photonics*, **5**, 48 (2018).
23. Desurvire E. *Erbium-Doped Fiber Amplifiers: Principles and Applications* (Wiley-Interscience, 2002).
24. Snyder A.W., Love J.D. *Optical Waveguide Theory* (London: Chapman and Hall, 1983; Moscow: Radio i Svyaz', 1987).
25. Akhmanov S.A., Vysloukh V.A., Chirkin A.S. *Optics of Femtosecond Laser Pulses* (New York: Am. Inst. of Physics, 1992; Moscow: Nauka, 1988).